Published in final edited form as:
Nanotechnology. 2012 May 4; 23(17): 175601. doi:10.1088/0957-4484/23/17/175601.

Confeito-like Assembly of Organosilicate-caged Fluorophores: Ultrabright Supranananoparticles for Fluorescence Imaging

Sangho Bok[1], **Venumadhav Korampally**[1], **Luis Polo-Parada**[2], **Vamsi Mamidi**[1], **Gary A. Baker**[3], **Keshab Gangopadhyay**[1,4], **William R. Folk**[5], **Purnendu K. Dasgupta**[6], and **Shubhra Gangopadhyay**[1]

[1]Department of Electrical Engineering, University of Missouri, Columbia, Missouri 65211, USA

[2]Department of Medical Pharmacology and Physiology, University of Missouri, Columbia, Missouri 65211, USA

[3]Department of Chemistry, University of Missouri, Columbia, MO 65211, USA

[4]Nanos Technologies, LLC. Columbia, Missouri 65203, USA

[5]Department of Biochemistry, University of Missouri, Columbia, Missouri 65211, USA

[6]Department of Chemistry and Biochemistry, University of Texas at Arlington, Arlington, Texas 76019-0065, USA

Abstract

We report ultrabright, photostable, sub-25 nm nanoparticle agglomerates (supranananoparticles) assembled from a few hundred 3.3 ± 0.9 nm units, each hosting on average a single rhodamine 6G (Rh6G) dye molecule encased in a thin organosilicate cage. These individual Rh6G-doped nanoparticle (DOSNP) units consist of a hydrophobic core containing the dye and an ultrathin, conformal silicate shell modified by CO_2 plasma to confer a beneficial "cage effect" as well as surface hydrophilicity. The isolation of the dye within individual DOSNP units in the final 22 ± 5 nm agglomerate avoids dimerization and related spontaneous molecular interactions that otherwise lead to self-quenching in closely co-localized fluorophores. The resulting supranananoparticles are over 200 times brighter than the free Rh6G molecules in the same volume. There is no observable dye leaching, and the labels are 20-fold more resistant to photobleaching than free Rh6G in solution. We demonstrate the attractive features of DOSNPs as labels in bioimaging applications.

1. Introduction

Fluorescent dyes are extensively used in biomedicine [1-5], from basic research to clinical diagnostics [6, 7] to contrast agents [8], also playing key roles in chem/bio threat sensors [1-3]. Fluorescent dyes do photobleach under continuous excitation, however [6, 9-11]. Luminescent quantum dots (QDs), which derive novel optical properties from quantum confinement effects [10, 12], are an efficient and photostable alternative [12, 13], but toxicity aspects of many QDs remain a concern [13-15]. Lower toxicity polyethylene glycol encapsulated QDs have been prepared, but the synthesis remains a challenge [16].

The approach of housing multiple dye molecules within a single nanoparticle can greatly increase the fluorescence signal compared to that arising from an isolated dye molecule [3, 5, 7, 11]. Furthermore, the matrix-confinement of the dye can protect the fluorophore from the external environment and improve photostability and biocompatibility [17]. Silica

gangopadhyays@missouri.edu.

remains the most popular choice as matrix because of its established biocompatibility, dispersibility in water, and the wide availability of commercial reagents. Preparation of silica nanoparticles is relatively straightforward; it is also readily scaled up using reverse microemulsion, and Stöber-type sol–gel approaches [18-20]. A reverse microemulsion is a surfactant-stabilized dispersion of nano-sized water droplets which can serve as versatile reactors for nanosynthesis, yielding uniform particle size. This approach also enables the incorporation of nonpolar dyes within hydrophilic silica. However, most such procedures result in leaky enclosures and, as a result, the fluorescence fades over time, a serious detriment both in terms of background (optical contrast) and potential toxicity. An alternative tactic is to covalently link the dye to a macromolecule to reduce leaking [18], although this adds considerable complexity to the process. The dye may also be conjugated with a hydrolyzable silica precursor [21] followed by a conventional sol–gel process, an approach that generally results in much larger particles [22].

Recently, Zhao et al. [5] reported a synthetic approach involving electrostatically binding a dye to a silica matrix which produced 60 nm nanoparticles containing multiple dye molecules per nanoparticle. Surfactants used during this synthesis can adversely affect biomembranes [5, 6], however, and extensive washing was needed to remove the surfactant. Cho et al. [24] reported the preparation of 40 nm nanoporous silica nanoparticles encaging Rh6G molecules in the porous channels, resulting in 30-fold brighter particles compared to comparably-sized QDs. In his process, dye leakage from the open channels was prevented by incorporation of hydrophobic groups in the silica matrix. However, the presence of hydrophobic groups resulted in a low zeta potential (+5 mV), limiting the long-term stability of the colloidal suspension of the particles. Another group reported on a two-step preparation of core-shell 20-30 nm dye-doped nanoparticles in which silica sol–gel monomers were added to a dense dye-rich 2.2 nm core to form a 15 nm shell [25]. The resulting core was less bright than the free dye, suggesting the occurrence of quenching. In this case, adding a silica shell greatly increased the fluorescence to a level 20 times that of the free dye. This “cage effect” was attributed to protection of the dye-rich core from solvent and reduction in losses from collisional relaxation [26], allowing for the achievement of QD-like brightness [27].

In the current work, we have developed bright, ultra-small dye-doped nanoparticle units (~3.3 nm) and 22 nm mesoscopic assemblies with excellent photo-physical characteristics and water solubility. Our process effectively addresses the extant problems associated with dye-doped nanoparticles in the following ways:

1. The problem of dye leakage from the nanoparticles under aqueous dispersion is mitigated through the formation of a core-shell structure; the dyes are encapsulated within a hydrophobic, organosilicate core that is surface functionalized with carboxyl moieties. This arrangement permits the material to be freely dispersed in water without leakage of the guest dye from the hydrophobic core.
2. Plasma-based surface modification is employed, affording a higher degree of control over the density and type of surface functionality introduced at the nanoparticle surface compared with conventional wet chemical means. For instance, the net surface charge on the nanoparticle can easily be controlled to achieve long-term aqueous dispersions.
3. During synthesis, nominally 3-nm unit particles are initially formed that ripen (assemble and cross-link) into suprananoparticles during aging (figure 1a). Each unit nanoparticle incarcerates a single dye molecule on average, which remains sequestered in an organosilicate cage, preventing deleterious self-quenching even when the unit colloids assemble into superstructures. Photobleaching is also curbed

by the presence of the silicate cage [28]. Each aggregated suprananoparticle, composed of ~200 "unit" particles, also contains about the same number of dye molecules (i.e., ~200) which, because they are present in isolation, are not subject to fluorescence quenching observed with dimer formation or other intermolecular interactions which spontaneously proceed at high local concentrations in the solution phase.

The concepts and steps guiding the synthesis of these nanoparticles derives from insight gained in our previous work [29] and can be summarized by figure 1. Non-crosslinked ~3 nm polymethylsilsesquioxane (PMSSQ) nanoparticles are initially formed in solution through polymer collapse in the presence of polypropylene glycol (PPG). The chemical structure of PMSSQ, which essentially consists of a siloxane backbone with pendant methyl and hydroxyl (OH) groups (~14% OH functionality), is key to the efficient dye encapsulation within the nanoparticles. Electrostatic attraction and hydrogen bonding between the spaced OH groups of PMSSQ and Rh6G molecules leads to dye adsorption in a monomeric state. These PMSSQ-wrapped dye molecules eventually become enveloped by a siliceous sheet as PMSSQ molecules conformational switch from a linear form to a compact globule one upon PPG addition. A dispersion of these PMSSQ-wrapped dyes is then spin cast to form a thin film; heating the film beyond the polymer decomposition temperature generates nanoporosity with crosslinking of the nanoparticle units [29].

In our approach, we directly incorporate Rh6G molecules within discrete PMSSQ nanoparticles during synthesis. Rendering the final suprananoparticles hydrophilic and based upon site-isolated dye units relies upon several aspects of the method: (i) Rh6G dye molecules electrostatically interacting with the PMSSQ moieties, promoting efficient entrapment during nanoparticle formation, (ii) ripening (increase in particle size) as the solution ages, associated with inter-particle crosslinking, (iii) spin casting of a thin film and thermal conversion to a nanoporous assembly of crosslinked suprananoparticles, and (iv) plasma-modification to efficiently functionalize the final particle surface, introducing hydrophilic groups allowing for wettability.

The extent of surface functionalization can be controlled by the plasma exposure parameters. After CO_2 plasma treatment, the suprananoparticle film is mechanically removed from the substrate by scraping under water. The recovered material is then sonicated to produce an aqueous dispersion of dye-doped suprananoparticles with carboxyl-functionalized surfaces. With limited sonication, the mean particle size of the dispersion is consistent with formation of primarily suprananoparticles, the integral unit of which is a hydrophobic organosilicate core containing the dye molecule and an ultrathin hydrophilic shell achieved by plasma oxidation. More aggressive sonication serves to liberate these individual units into these core-shell nanostructures.

Herein, we report the details of our synthesis and characterization of water-soluble suprananoparticles incorporating site-isolated Rh6G dye (quantum yield ~0.95). We examine both 3.3 ± 0.9 nm DOSNPs each containing on average one to three Rh6G molecule (herefrom referred to as 3.3 nm particles) as well as 22 ± 5 nm suprananoparticles assembled from the unit DOSNP nanoparticles (hereafter, simply 22 nm suprananoparticles). It is noteworthy that no fluorescence quenching behavior was observed for the unit 3.3 nm particles, making them the smallest luminescent dye encapsulated (core-shell) nanoparticle reported to date. Although these nanoparticles were observed to be only slightly more fluorescent than the free dye molecule itself, their superior photophysical characteristics and small sizes (on the order of the size of the dye molecules themselves) makes them an attractive alternative for fluorescent dyes for single-molecule studies and other fundamental research requiring the long-term observation of fluorescence events [28]. The utility of this novel class of luminescent nanoparticles is further illustrated with a

fluorescence imaging experiment that shows the distribution of fibronectin, a high-molecular weight (~440 kD) dimeric extracellular glycoprotein, in embryonic chicken hearts.

2. Experimental methods

2.1. Materials and reagents

Polymethyl silsesquioxane (PMSSQ, M_w = 10,000; 14% hydroxyl groups) and Rh6G were from Techneglas, Inc. (P/N GR650F) and Exciton (Dayton, OH), respectively. Polypropylene glycol (PPG, M_n = 425), 2-(N-morpholino)ethanesulfonic acid hydrate (MES), bovine serum albumin (BSA) and phosphate buffered saline, pH 7.4 (PBS) were from Sigma-Aldrich (St. Louis, MO). N-(3-Dimethylaminopropyl)-N-ethylcarbodiimide hydrochloride (EDC), N-Hydroxysulfosuccinimide sodium salt (sulfo-NHS), and hydroxylamine hydrochloride (HA-HCl) were from Pierce Biotechnology and used for the conjugation of antibodies to the nanoparticles. Suprananoparticles were conjugated to Goat anti-mouse antibodies (Jackson Immunoresearch Laboratories, Inc.). The antifibronectin antibody (B3/D6) was from the Developmental Studies Hybridoma Bank developed under the auspices of the National Institute of Child Health and Human Development (NICHD) and maintained by the University of Iowa, Department of Biological Sciences (Iowa City, IA).

2.2. Hydrogen-passivated silicon substrate

Hydrogen passivation was achieved by dipping the Si substrates in 10 wt% aqueous HF solution for > 30 s prior to film deposition (spin casting @ 3000 rpm, 30 s).

2.3. DOSNP preparation

PMSSQ and Rh6G (mass ratio ~ 62) were dissolved in ethanol. Polymer collapse was initiated by the addition of a low molecular weight PPG (M_n = 425), a poor solvent [30-32]. Total 10 grams were typically prepared in a 20mL glass vial with aging for 3 days in the dark at room temperature. Films were spin-cast on hydrogen-passivated low doped p-type Si substrates from the solution with weight composition PMSSQ:PPG:ethanol 1:1:2. Films were immediately calcined (put on hot plate at 250 °C, 35 s) removed and allowed to cool. The calcined film was then treated by a CO_2 plasma (see next section). Particle suspensions were made from the nanoparticle films without light exposure. The carboxylated films were soaked in water (5 min) and then extensively water-washed to remove free Rh6G. The films were then scraped off the substrate, while still immersed in water, using a scalpel blade. The nanoparticulate flakes in water were put in a low-power ultrasonic bath for 30 min and filtered through a 0.2 μm filter. The clear solution contained confeito-shaped suprananoparticles. Higher power sonication (sonic wand, 50 W) resulted in complete disintegration within 10 min to the original 3.3 nm unit spheres.

2.4. Carbon dioxide plasma treatment

A custom built plasma enhanced chemical vapor deposition (PECVD) system (MV Systems Inc., Golden, CO) was used for the CO_2 plasma treatment. The following conditions were used for the plasma treatment: working pressure, 510 mTorr; CO_2 flow rate, 50 sccm; power, 20 W; and plasma treatment time, 10 min. These conditions were found to be optimal as lower power and shorter plasma treatment times failed to induce sufficient carboxylation/hydrophilicity whereas higher powers and longer exposures times damaged the material, decreasing photostability.

2.5. Sonication

For low power sonication we used a Cole-Parmer model 8890 ultrasonic bath. For higher sonication intensity, a sonic wand (Sonics & Materials Inc., Model VCX130; 50 W) was used.

2.6. Antibody-DOSNP conjugation

Carbodiimide-mediated chemistry [33] was used to couple antibodies with carboxylate-functionalized suprananoparticles. Briefly, 0.4 mg EDC, 1.1 mg sulfo-NHS, and 3 mg suprananoparticles were combined in 1 mL of activation buffer (0.1 M MES, 0.5 M NaCl, pH 6.0) and stirred in the dark for 15 min. Next, 1 mg of anti-mouse antibody was added and the pH carefully adjusted to 8 with addition of dilute NaOH. After gently agitating for 2 h at room temperature, the reaction was quenched by the addition of 10 mM HA-HCl.

2.7. Chick heart tissue preparation for imaging

Embryonic chicken hearts were extracted from the embryos of 3 to 4 day-old incubated eggs at 37 °C and dehydrated by soaking successively in 70, 80, 90, and then 100% ethanol for at least 5 min at each condition. Dehydrated hearts were soaked in xylene and then submerged in melted paraffin at 70 °C. The hearts were paraffinized overnight and then microtomed to 5 μm thicknesses. The tissue slices were placed on a glass slide and deparaffinized by soaking in neat xylene followed by 10 min each in 90, 80, and then 70% xylene. The glass slide was then placed for 10 min apiece in 99, 90, 80, and 70% ethanol and finally in distilled water. The deparaffinized tissue slices were dried overnight at room temperature and then a citrate buffer antigen retrieval protocol (10 mM citric acid, 0.05% Tween® 20, pH 6.0) was used to unmask the antigens and epitopes in the paraffin embedded tissue sections, thus permitting efficient attachment by tagged antibodies. A microwave was used instead of a steamer or water bath [34]. After room temperature overnight drying, the slides were stored at −20 °C prior to experimentation.

The chick heart slides were blocked with 1% BSA for 30 min followed by the addition of antifibronectin antibody. The slides were incubated overnight at 4 °C, followed by three repeated washing with PBS for 5 min each time to remove excess antibody. The chick heart tissues thus prepared were exposed to suprananoparticles conjugated with anti-mouse antibodies and incubated for 3 h at room temperature followed by repeated washing with PBS (3×, 5 min each). As a control experiment, chick heart tissue samples were exposed to suprananoparticles and incubated for 3 h at room temperature followed by washing with PBS for 5 min three consecutive times. Finally, the slides were imaged using a fluorescence microscope.

2.8. Photostability measurements and fluorescence imaging

The photostability of the suprananoparticle dispersion in water was evaluated with a fluorescence microscope (Olympus BX51WI) equipped with a 130 W xenon lamp. A circular well (8 mm diameter) was prepared in polydimethylsiloxane and 10 μL of the dye/nanoparticle dispersion in water was placed therein. The well was covered with a thin glass slide to prevent water evaporation loss. A FITC filter set (bandpass excitation filter (475 nm center, 28 nm halfwidth); long pass emission filter (50 % T @ 515 nm); dichroic mirror cut-on wavelength: 500 nm; Semrock, Rochester, NY) was used. The samples were observed using a 10× lens (Olympus America, Melville, NY); the illumination flux at the sample surface was measured to be 21 mW/cm^2. The fluorescence was intensity was read by a fiber optic coupled CCD spectrometer (USB-4000, Ocean Optics, Dunedin, FL). Spectra were taken as a function of time while the sample was continuously illuminated. Steady-state emission and excitation profiles of the suprananoparticle dispersion in water were measured

with a FluoroLog-3 spectrofluorometer (Horiba Jobin Yvon (IBH)). The chicken heart tissues were imaged with a TRITC-A filter set (bandpass excitation filter (543 nm center, 22 nm halfwidth); long pass emission filter (50 % T @ 575 nm); dichroic mirror cut-on wavelength: 570 nm; Semrock, Rochester, NY) and a 10x lens.

2.9. Size characterization

The material at various stages was characterized as follows. Dynamic light scattering (DLS, model LB-550, Horiba Jobin Yvon (IBH)) was used to characterize the initially formed uncrosslinked nanoparticles in the precursor solution. The laser excitation wavelength (630 nm) did not overlap with the excitation wavelength of the dye. 100 individual measurements were averaged to obtain the size data. Atomic force microscopy (AFM, Model 550, Agilent Technologies) was used to characterize the nanoporous thin film after calcination. AFM scans were performed in the tapping mode with silicon cantilevers (VP40148, VISTA probes, mean tip radius <10 nm). Transmission electron microscopy (JEOL-1400) was used with an acceleration voltage of 120 kV to characterize the size and the morphology of the suprananoparticles.

2.10. Fourier transform infrared (FTIR) spectroscopy

Transmission mode infrared spectra of the nanoparticle films supported on the silicon wafers were collected on a Nicolet-4700 FTIR spectrometer.

2.11. Measurement of zeta potential

The zeta potential measurements of DOSNPs were performed on Delsa Nano HC (Beckman Coulter Inc., United States). The DOSNPs (100 μg) were dispersed in DI water (3 mL). Average values for the zeta potential were determined with at least three repeat measurements with ten runs per sample.

2.12. Fluorescence lifetime measurement

Time-resolved fluorescence experiments were carried out by using a Horiba Jobin Yvon (IBH) model 5000F time-correlated single-photon-counting (TCSPC) fluorescence lifetime instrument equipped with a picosecond detection module (TBX-04). A 460 nm pulsed light emitting diode (NanoLED, IBH) with a 1.2 ns pulse width was used as the excitation source. The emission monochromator was set at 562 nm with a spectral band-pass of 8 or 12 nm. To avoid pulse pileup, detector count rates was always maintained below 2% of the NanoLED repetition rate (1 MHz). The instrument response function and the fluorescence intensity decay traces were recorded under magic angle polarization conditions. In a typical experiment, the instrument response function was obtained from a nominally 80-nm size colloidal silica suspension in ethanol prepared in house using a modified Stöber sol–gel process. The typical time resolution of the instrument was 56.4 ps/channel, on a 1024-channel analyzer. A dilute solution of either fluorescein in aqueous KOH ($\tau_{ref} = 4.00 \pm 0.02$ ns) or Rh6G in ethanol ($\tau_{ref} = 3.85 \pm 0.01$ ns) were used as a reference lifetime standards [42]. Experiments were conducted until $>10^4$ counts accumulated in the peak MCA channel. Decay analysis and curve fitting routines were performed using manufacturer-supplied software or an independent package (Globals WE, Globals Unlimited, Urbana, IL).

3. Results and discussion

3.1. Physical and Chemical Characteristics

Dynamic light scattering measurements of the uncrosslinked DOSNP suspension showed a gradual increase in particle size over time. Aging for 3 days increased the mean size of these uncrosslinked particles to 34 ± 12 nm. Aging for a smaller period was observed to form

smaller agglomerates while t > 4 days resulted in complete gelation. Figure 2a shows the AFM image of the film surface obtained by spin-casting the 3-day aged solution and calcination (250 °C, 35 s). The calcination temperature and duration was optimized to achieve effective decomposition of PPG molecules and formation of the film with sufficient nanoporosity while preventing undesirable decomposition of the encapsulated dye molecules.

From figure 2a, it can be seen that the individual nanoparticles have an apparent mean diameter of 50 nm; correction for the finite ~10 nm tip size indicates an actual particle size of 20–30 nm. The film surface is remarkably smooth with ~2 nm rms roughness. Figures 2b and 2c shows the TEM images of the particles obtained from the plasma surface functionalized film by scraping under DI water followed by different sonication conditions. Under mild sonication, suprananoparticles of 22 ± 5 nm mean diameter were obtained (figure 2b and 2d); the morphology is confeito-like, similar to that previously observed for galvanically formed gold nanostructures [35]. Intense sonication fragmented the agglomerates into individual unit nanoparticles of mean diameter 3.3 ± 0.9 nm (figure 2c and 2e). The latter particles did not aggregate when dispersed in deionized water, indicating that the particle surfaces were likely sufficiently carboxylated by plasma treatment resulting in inter-particle Coulombic repulsion. Furthermore, zeta potentials of the unit particles and the suprananoparticles in DI water were measured to be −19.3 ± 2.9 mV and −16.1 ± 1.0 mV respectively; large enough to maintain the stability of the colloidal suspension of the particles [36].

Plasma surface modification has an important bearing on the nanoparticle physico-chemical characteristics and had to be carefully optimized to achieve nanoparticles with the desired attributes. The plasma conditions were optimized to induce sufficient carboxylation of the nanoparticle surfaces while maintaining the molecular structure integrity of the nanoparticle cores. In this regard, CO_2 plasma was found to be less harsh affording a greater control on the surface characteristics of the nanoparticles. In contrast, use of O_2 plasma led to rapid degradation of the nanoparticles that was manifested as dramatically reduced photostabilities of the exposed nanoparticles. Figure 3 shows the FTIR spectra of the porous dye doped nanoparticulate film before and after the CO_2 plasma treatment. The spectra contain peaks characteristic of PMSSQ films: notably, 2975 cm^{-1} (CH_3 asymmetric stretching), 1420 cm^{-1} (CH_3 bending), 1275 cm^{-1} (–Si–CH_3 stretching), 845 cm^{-1} (–Si–$(CH_3)_2$ bending), and 775 cm^{-1} (–Si–CH_3 bending). After 10 min of CO_2 plasma treatment, the C=O asymmetric stretching vibration from the CO_2H groups around 1720 cm^{-1} can be readily seen, indicating carboxylation of the paticles [37]. All other peaks, particularly the Si–CH_3 stretching near 1275 cm^{-1} remain unchanged, indicating that the plasma does not otherwise affect the particles. A broad O–H peak around 3450 cm^{-1}, attributed to adsorbed moisture within the porous network, can also be seen after plasma treatment. The presence of both $SiCH_3$ and –CO_2H groups is notable: the former abundantly present within the core effectively prevent the penetration of moisture into the nanoparticle core while surface –CO_2H groups allow hydrophilicity and aqueous dispersibility.

3.2. Fluorescence Characteristics of the Nanoparticles

The fluorescence brightness of the unit nanoparticles and suprananoparticles (FL_{DOSNP}) relative to the brightness of a single Rh6G molecule was measured as follows, following the procedure reported by Cho *et. al* [24]:

$$FL_{DOSNP} = \frac{I_{DOSNP}/C_{DOSNP}}{I_{Rh6G}/C_{Rh6G}} \quad (1)$$

where I_{DOSNP} and I_{Rh6G} are the measured fluorescence intensities of the stock solutions of the DOSNPs and Rh6G solutions respectively. C_{DOSNP} and C_{Rh6G} are the respective concentrations of the DOSNP (number of DOSNPs/unit volume) and Rh6G (number of dye molecules/unit volume) stock solutions. To obtain the values of C_{DOSNP}, mass of the particles present in 1 ml stock solution was first obtained by evaporating the entire solution using a rotoevaporator and measuring the weight of the resulting solid using a high resolution weighing balance. Taking the average diameter of the nanoparticles (3.3 nm for unit nanoparticles and 22 nm for suprananoparticles and assuming them to be spherical), and known density of PMSSQ – 1.08 g/cm^3 [38], the number of particles present in the stock solution was calculated. Following this procedure, C_{DOSNP} for the unit nanoparticles and the suprananoparticles were calculated to be 9.25×10^{14} and 2.96×10^{12}, respectively. The measured fluorescence intensities of the stock solutions were $1.17 (\pm 0.11) \times 10^7$ au and $0.75 (\pm 0.03) \times 10^7$ au for the unit nanoparticles and suprananoparticles, respectively. The fluorescence of Rh6G solution was measured to be $5.45 (\pm 0.23) \times 10^6$ au from a 0.36 μg/ml (corresponding to 4.53×10^{14} molecules/ml) solution. From these values, using equation (1), relative brightness of a single unit nanoparticle and suprananoparticle was calculated to be equal to the brightness of 1.05 ± 0.1 and 212 ± 9.7 molecules of Rh6G, respectively. The fluorescence of each suprananoparticle further corresponds to about 10 times the brightness of a single CdSe quantum dot (a single CdSe QD is reportedly as bright as 20 Rh6G molecules [27]). It should be noted that quantum yields of QD and Rh6G are 0.35 ~ 0.5 and 0.95, respectively. Recent improvements in synthesis techniques however led to realization of QDs with quantum yields as high as 0.65-0.85 [39]. Taking this into account, the relative fluorescence brightness of the DOSNPs to these QDs is calculated to be ~ 5. Figure 4 summarizes the relative fluorescence intensities per nanoparticle as related to the fluorescence intensity of a single Rh6G dye molecule. From the relative fluorescence intensity values of the unit nanoparticles and the suprananoparticles, it can be concluded that each suprananoparticle essentially is an aggregated structure consisting of ~ 200 unit nanoparticles. This value matches well with the theoretically estimated value using geometric random close packing model consideration as the model calculates that 64% of the volume of a large sphere (22 nm diameter) can be occupied by small spheres of 3.3 nm diameter [40]. Therefore, for a 22 nm suprananoparticle, this corresponds to a packing of ~ 200 unit nanoparticles (3.3 nm diameter) matching well with our experimentally derived value.

Fluorescence excitation and emission spectra of the nanoparticles are shown in figure 5. It may be observed that the spectra of the unit nanoparticles and the suprananoparticles are identical. Rh6G and Rh6G bearing nanoparticles in water show excitation/emission peaks at 531/554 nm and 520/542 nm, respectively. These blue shifts are typical for dye-doped nanoparticles and are believed to arise from “cage effects” [26]. This shift may also be due to a reduction in the dipole moment of the Rh6G; the normally solvated region is confined within the cage. A reduction in solvent polarity for dyes in solution results in hypsochromic shift in the emission spectrum ($\lambda_{em,max}$ decreases) [26]. If dimers are formed (common when two dye molecules come in close proximity, particularly at surfaces [41, 42]), the emission band is red shifted. This was notably absent; the conformal organosilicate shells likely prevent such interaction and suggest that there is no quenching even though the dye molecules are brought into such close proximity. In contrast, others have reported very significant self-quenching of fluorescence when multiple dye molecules were incorporated in nanoparticle core structures [6, 24, 25]. The present results indicate that formation of clusters from well-protected unit DOSNPs may be a valuable new means to incorporate many dye molecules in a single particulate tag without self-quenching. This was further corroborated by the quantum yield measurements of the dye-doped nanoparticles.

Quantum yield (QY) of the suprananoparticles were calculated as follows [23]:

$$QY = 0.95\left(\frac{Grad_{DOSNP}}{Grad_{Rh6G}}\right)\left(\frac{n_{DOSNP}}{n_{Rh6G}}\right)^2 \quad (2)$$

where *Grad* is the slope of the integrated fluorescence intensity versus absorbance gradient for the aqueous DOSNP dispersion ($Grad_{DOSNP}$) and Rh6G solution ($Grad_{Rh6G}$), respectively, from five different concentrations considered (40, 80, 120, 160 and 200ng mL^{-1} for DOSNP; 0.48, 0.96, 1.44, 1.92 and 2.4 μg mL^{-1} for Rh6G) (figure 6); in equation (2), $n_{DOSNP} = n_{Rh6G}$ are the refractive indices of the solvent (water) and 0.95 is the quantum yield of Rh6G [24]. Using equation (2), the quantum yield of the suprananoparticles was computed to be 0.99 ± 0.10. Therefore, within the error of the measurement, the quantum yields of the suprananoparticle-encapsulated Rh6G and free Rh6G in water are identical, further validating that dye dimerization was indeed absent in the suprananoparticles.

Figure 7 presents typical fluorescence intensity decay profiles for molecular Rh6G and Rh6G-doped suprananoparticles, both in water. Both decays were rigorously described by a single-exponential decay models. The goodness-of-fit is confirmed by the near-unity chi-square value (χ^2~1.16), the lack of improvement in χ^2 if a double-exponential decay model is invoked, and the randomness of the residuals about zero (figure 7b). Rh6G has an excited-state lifetime near 3.85 ns in both water and lower alcohols [43]. One report suggests that when a molecule is confined in a small nanoparticle (2.2 nm), fluorescence lifetime decreases due to self-quenching and nonradiative energy transfer to surface defects [6]. On the other hand, if the dye concentration is high, as in sol-gel-derived silica gels with high concentrations of Rh6G, there is a progressive red shift of the emission spectra to 567 nm with increasing Rh6G concentration due to dimer formation. This is accompanied by significantly longer lifetimes (up to 5.9 ns) associated with J-dimer species adsorption onto porous silica walls [42].

Here, we observe no change in the emission maximum. Aside from the lack of self quenching as observed from the intensity measurements, the lifetimes increase marginally from 3.82 ± 0.02 ns (Rh6G in ethanol) to 3.93 ± 0.01 and 4.05 ± 0.02 ns for the unit nanoparticle and the suprananoparticle, respectively. Note that previous efforts successfully achieved dye immobilization inside pores and achieved high fluorescence intensities per particle but these were micron-scale structures [44], impractical for bioimaging. The present method permits multiple silicate-wrapped dyes in monomeric form in a nanoassembly and such suprananoparticles can demonstrably provide ultrabright bioimaging labels.

It is well known that effective encapsulation of fluorescent dye molecules within inert matrices significantly enhances the photostability of the dye molecules [17]. The photostabilities of Rh6G and Rh6G-containing 3.3 nm unit nanoparticles and 22 nm suprananoparticles were compared in water where the optical densities of these fluorophores were same (see figure 8). In all cases, a first-order decay was observed. Correlation coefficients (r^2) for log fluorescence intensity versus time were 0.959, 0.994, and 0.993, respectively. Half-lives under under continuous illumination (475 nm/28nm, 26 mW cm^{-2}) illumination were 0.5, 7.1, and 6.4 h, respectively. The unit nanoparticle and the suprananoparticle are a decade more resistant compared to free Rh6G. To further prove that the encapsulation of the dye with organosilicate matrix is responsible for the enhanced photostabilities, we have also studied the photostability of Rh6G molecules physically adsorbed on suspended, non fluorescent organosilicate nanoparticles. Organosilicate nanoparticles devoid of dye were prepared and surface functionalized using the similar processes employed for DOSNP synthesis, however without the addition of the Rh6G molecules during synthesis.

The nanoparticulate films following CO_2 plasma treatment were soaked in 1mM Rh6G solution for 1 hour and washed multiple times with deionized water until no fluorescence was observed in the washed solution. These nanoparticles (Rh6G adsorbed nanoparticles) were then scraped, suspended in DI water and tested for their photostability. It can be seen from figure 8, the photostability of these nanoparticles closely followed that of free rhodamine dye molecules dissolved in DI water supporting that encapsulating dye molecules in the non-polar organosilicate cage is indeed responsible for enhanced photostability of the DOSNPs.

3.3. Bioconjugation of Suprananoparticles and Tissue Imaging

Fluorescence imaging of tissues and cells are an important aspect of biomedical research and are routinely performed using fluorescent dye labeled antibodies. In these applications, increasing the number of fluorophore molecules attached to a single antibody translates to higher signal to noise ratio images and a reduction in concentrations of the antibodies needed. However, it is imperative that this increase in the number of fluorophores/antibody minimally affect the natural activity of the antibodies. Ultra bright nanoparticles encapsulating hundreds of dye molecules are especially attractive for these applications. A single bound nanoparticle increases the signal sensitivity many fold compared to bound fluorescent dyes.

Figures 9 a–d show the fluorescence and reflected light optical micrographs of fibronectin in chick heart tissue upon conjugation with the Rh6G containing suprananoparticles and DyLight 549. The nonspecific binding of suprananoparticles to tissue was minimized by blocking the tissue with a 1% BSA solution for 30 min. When suprananoparticles were applied to the chick heart tissue with blocking, no significant staining was observed (figures 9e and 9f). DyLight 549 was used as a comparison benchmark fluorescent dye. For a direct comparison, labeled antibodies were characterized in terms of degree of substitution (DOS) [45] that represents the number of dye molecules attached to each single antibody. Following antibody labeling and purification, DOS was computed as follows:

$$DOS = \frac{[Dye]}{[Antibody]} \tag{3}$$

where [Dye] and [Antibody] are the molar concentrations of dye and antibodies respectively, obtained from the optical absorption measurements of the conjugates. Respective molar concentrations were calculated as

$$[Dye] = \frac{A_{dye} \times D_{dye}}{\varepsilon_{dye}} \tag{4}$$

where A_{dye} is the absorbance of the dye at the wavelength of maximum absorption (λ_{max}; for Rh6G, λ_{max} = 521 nm; for Dylight 549, λ_{max} = 562nm), ε_{dye} is the extinction coefficient of the dye at λ_{max} (ε_{Rh6G} = 88,147 M^{-1} cm^{-1} and ε = 150,000 M^{-1} cm^{-1}) and D is the dilution factor ($D_{dye} = D_{antibody}$ = 10 in the experiment). Molar concentration of the antibody was determined by:

$$[Antibody] = \frac{\left(A_{Ab} - C \times A_{dye}\right) \times D_{antibody}}{\left(\varepsilon_{Ab}\right)} \tag{5}$$

where A_{Ab} is the observed absorbance at 280 nm wavelength (corresponding to the absorption from the antibodies and the dyes), the product $C \times A_{dye}$ accounts for the

absorption of the dye at 280 nm. *C* is calculated as the ratio of the molar absorptivity of the dye at 280 nm to that at its λ_{max} (For Rh6G, *C* = 0.243 and for Dylight 549, C = 0.081).

From the DOS calculations, it was determined that on average, 4 Dylight 549 molecules and 64 Rh6G molecules (in the form of the suprananoparticles) were respectively attached to each goat antimouse antibody. The apparent disparity in the measured DOS and the number of dye molecules per suprananoparticle suggest that a suprananoparticle, with multiple binding sites, shares ~3 antibody molecules on the average. The lower calculated DOS may also arise due to the co-existence of 3.3 nm particles within the dispersion thereby reducing the average fluorescence intensity per conjugated antibody. At the same antibody concentration, the Dylight 549 labeled antibody produced a far dimmer image than the suprananoparticle labeled antibody. To ensure that it is not a failure of the Dylight-labeled antibody to attach, we used a 1,900 nM concentration of Dylight 549 labeled antimouse antibody (figure 10a) and compared this again with another staining experiment with 3 nM Rh6G-containing suprananoparticle labeled antibody (figure 10b). Images of more comparable brightness were now obtained with this 640× higher Dylight labeled antibody concentration.

4. Conclusions

We have developed a facile method for generating dye-centered, individually-caged nanoparticle building blocks and their stable crosslinked suprananoparticle assemblies. The particle surface was hydrophilized by plasma treatment, making them water-dispersible and subject to subsequent functionalization. Extant problems of dye leaching and quenching due to dimerization were solved through the unique core-shell organosilicate structures and suprananoparticle assemblies respectively. The suprananoparticles provide attractive fluorescence tags for bioimaging and chemosensory applications, exhibiting photostable, ultrabright emission. Given the palette of molecular dyes amenable to this approach, and the fact that particle size and surface chemistry appear tunable, these new nano-emitters suggest the promise of devising a new generation of ultrabright tags toward numerous ends.

Acknowledgments

We gratefully acknowledge financial support from Tibotec REACH, National Institutes of Health (R90DK071510), and the National Science Foundation (CHE-0821969). We also thank the Developmental Studies Hybridoma Bank for providing the anti-fibronectin antibody B3/D6 generated by Fambrugh, D. M. developed under the auspices of the NICHD and maintained by The University of Iowa, Department of Biology, Iowa City, IA 52242.

REFERENCES

(1). Nagasawa S, Shimoyama I. Sensor Actuat B-Chem. 2004; 102:7–13.

(2). Qin D, He X, Wang K, Zhao XJ, Tan W, Chen J. J. Biomed. Biotechnol. 2007; 2007:89364. [PubMed: 18273415]

(3). Santra S, Wang K, Tapec R, Tan W. J. Biomed. Opt. 2001; 6:160–6. [PubMed: 11375725]

(4). Tapec R, Zhao XJ, Tan W. J. Nanosci. Nanotechnol. 2002; 2:405–9. [PubMed: 12908270]

(5). Zhao X, Bagwe RP, Tan W. Adv. Mater. 2004; 16:173–6.

(6). Burns A, Owb H, Wiesner U. Chem. Soc. Rev. 2006; 35:1028–42. [PubMed: 17057833]

(7). Lian W, Litherland SA, Badrane H, Tan W, Wu D, Baker HV, Gulig PA, Lim DV, Jin S. Anal. Biochem. 2004; 334:135–44. [PubMed: 15464962]

(8). Santra S, Bagwe RP, Dutta D, Stanley JT, Walter GA, Tan W, Moudgil BM, Mericle RA. Adv. Mater. 2005; 17:2165–9.

(9). Chan WC, Maxwell DJ, Gao X, Bailey RE, Han M, Nie S. Curr. Opin. Biotechnol. 2002; 13:40–6. [PubMed: 11849956]

(10). Santra S, Zhang P, Wang K, Tapec R, Tan W. Anal. Chem. 2001; 73:4988–93. [PubMed: 11681477]
(11). Yan J, Estevez MC, Smith JE, Wang K, He X, Wang L, Tan W. Nanotoday. 2007; 2:44–50.
(12). Lee KH. J. Nucl. Med. 2007; 48:1408–10. [PubMed: 17785725]
(13). Henglein A. Chem. Rev. 1989; 89:1861–73.
(14). Alivisatos AP. Science. 1996; 271:933–7.
(15). Baker SN, Baker GA. Angew. Chem. Int. Ed. 2010; 49:6726–44.
(16). Yu WW, Chang E, Drezek R, Colvin VL. Biomed. Biophys. Res. Comm. 2006; 348:781–6.
(17). Kim HK, Kang SJ, Choi SK, Min YH, Yoon CS. Chem. Mater. 1999; 11:779–88.
(18). Baker GA, Watkins AN, Pandey S, Bright FV. Analyst. 1999; 124:373–9.
(19). Stöber W, Fink A, Bohn E. J. Coll. Interfac. Sci. 1968; 26:62–9.
(20). Ye Z, Tan M, Wang G, Yuan J. J. Mater. Chem. 2004; 14:851–6.
(21). Pandey S, Baker GA, Kane MA, Bonzagni NJ, Bright FV. Chem. Mater. 2000; 12:3547–51.
(22). van Blaaderen A, Vrij A. J. Coll. Interfac. Sci. 1993; 156:1–18.
(23). Williams ATR, Winfield SA, Miller N. Analyst. 1983; 108:1067–71.
(24). Cho E, Volkov DO, Sokolov I. Small. 2010; 6:2314–9. [PubMed: 20859948]
(25). Ow H, Larson DR, Srivastava M, Baird BA, Webb WW, Wiesner U. Nano Lett. 2005; 5:113–7. [PubMed: 15792423]
(26). Anedda A, Carbonaro CM, Clemente F, Corpino R, Grandi S, Magistris A, Mustarelli PC. J. Non-Cryst. Solids. 2005; 351:21–3.
(27). Chan WCW, Nie S. Science. 1998; 281:2016–18. [PubMed: 9748158]
(28). Trenkmann I, Tauber D, Bauer M, Schuster J, Bok S, Gangopadhyay S, von Borczyskowski C. diffusion-fundamentals.org. 2009; 11:108.diffusion-fundamentals.org
(29). Korampally V, Yun M, Rajagopalan T, Dasgupta PK, Gangopadhyay K, Gangopadhyay S. Nanotechnol. 2009; 20:425602–8.
(30). Raos G, Allegra G. J. Chem. Phys. 1997; 107:6479–90.
(31). Williams C, Brochard F, Frisch HL. Annu. Rev. Phys. Chem. 1981; 32:433–451.
(32). Yabu H, Higuchi T, Ijiro K, Shimomura M. Chaos. 2005; 15:047505. [PubMed: 16396598]
(33). Hermanson, GT. Bioconjugate Techniques. NY Academic Press; New York: 2008. p. 219-23.
(34). Tacha DE, Chen T. Histotechnology. 1994; 17:365–6.
(35). Sharma J, Tai Y, Imae T. J. Phys. Chem. C. 2008; 112:17033–7.
(36). American Society for Testing and Materials. ASTM Standard D. 1985:4187–82.
(37). Dixit, SG.; Vanjara, AK. Polymer Interfaces and Emulsions. Esumi, K., editor. NY Marcel-Dekker, Inc.; New York: 1999. p. 381-3.
(38). Wei Q, Pippel E, Woltersdorf J, Scheffler M, Greil P. Mater. Chem. Phys. 2002; 73:281–9.
(39). Resch-Genger U, Grabolle M, Cavaliere-Jaricot S, Nitschke R, Nann T. Nature Methods. 2008; 5:763–75. [PubMed: 18756197]
(40). Song C, Wang P, Makse HA. Nature. 2008; 453:629–32. [PubMed: 18509438]
(41). del Monte F, Levy D. J .Phys. Chem. B. 1998; 102:8036–41.
(42). del Monte F, Mackenzie JD, Levy D. Langmuir. 2000; 16:7377–82.
(43). Watkins AN, Ingersoll CM, Baker GA, Bright FV. Anal. Chem. 1998; 70:3384–96. [PubMed: 9726164]
(44). Sokolov I, Kievsky YY, Kaszpurenko JM. Small. 2007; 3:419–23. [PubMed: 17245779]
(45). Brinkley M. Bioconjugate Chem. 1992; 3:2–13.

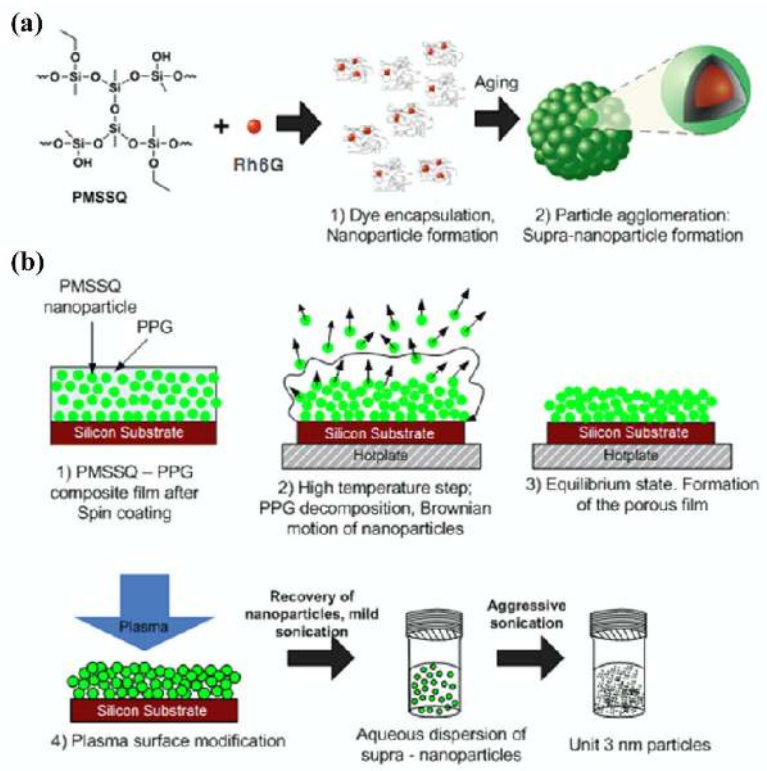

Figure 1.

Schematic illustration of the dye-doped organosilicate nanoparticle synthesis. (a) Solution phase synthesis of uncrosslinked nanoparticles and the supranananoparticle architecture of the nanoparticles. (b) Nanoporous film formation and formation of water soluble nanoparticles.

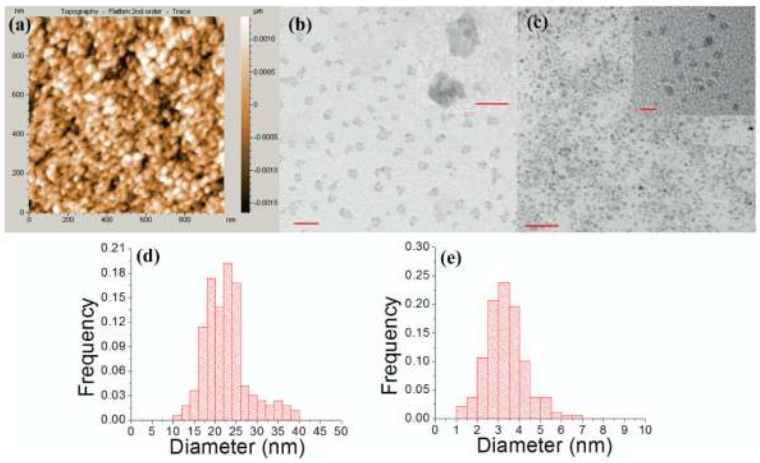

Figure 2.

DOSNP images. (a) AFM image of a DOSNP nanoparticulate film. (b) TEM image of confeito-shape suprananoparticles obtained after mild ultrasonication (inset: zoomed view) (c) TEM image of unit nanoparticles obtained after intense ultrasonication (inset: zoomed view); scale bar is 50 nm. Scale bars of insets are 5 nm and 20 nm for (b) and (c), respectively. (d) size distribution of confeito-shape suprananoparticles. (e) size distribution of unit nanoparticles.

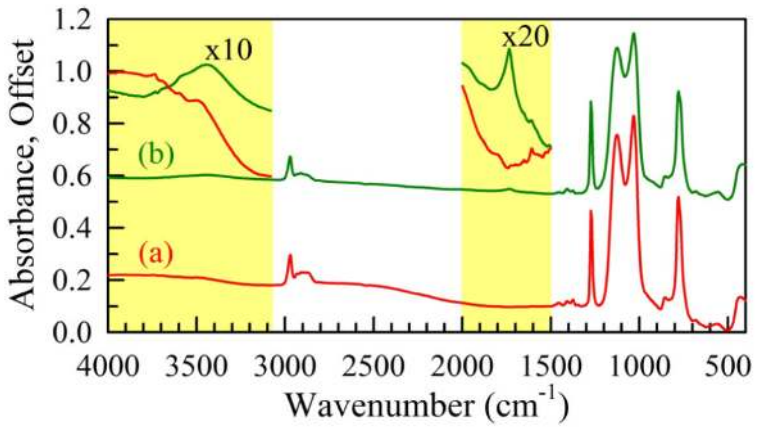

Figure 3.

FTIR spectra of DOSNP films before and after a 10 min CO_2 plasma treatment at 20 W. Inset is a zoomed view of the asymmetric stretching vibration of C=O in CO_2H groups around 1720 cm^{-1}. Post-plasma appearance of the band around 3450 cm^{-1} attributed to water sorption is also notable.

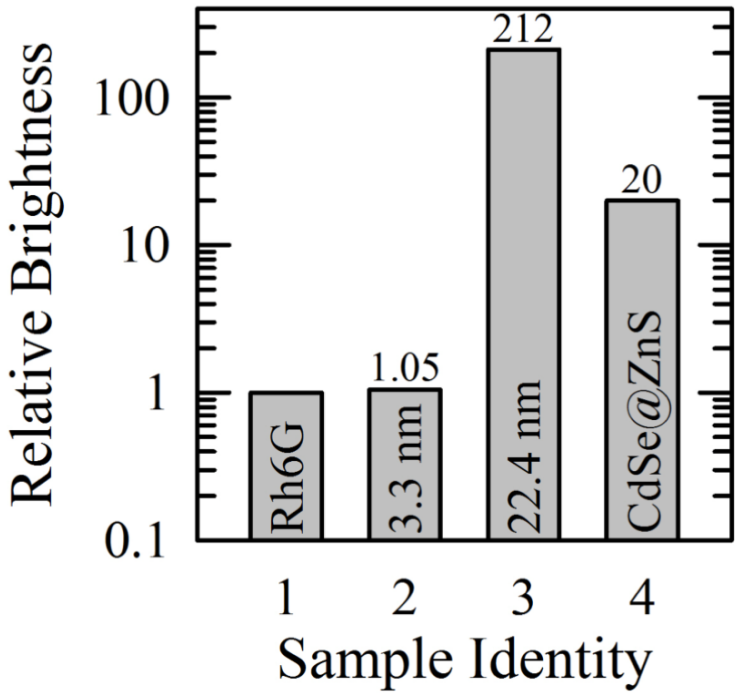

Figure 4.
Comparison of fluorescence intensities (one particle or one molecule) for (1) Rh6G, (2) single Rh6G-containing nanoparticles, (3) DOSNP suprananoparticles, and (4) CdSe@ZnS QDs.

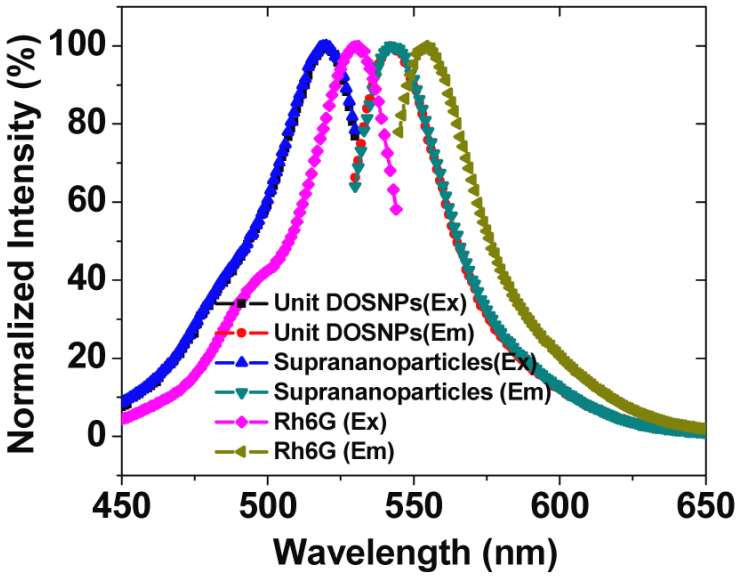

Figure 5.
Normalized excitation and emission spectra for unit DOSNPs, 22.4 nm suprananoparticles and Rh6G all in water. As can be seen, the spectra measured for the unit DOSNPs and the suprananoparticles in water are indistinguishable.

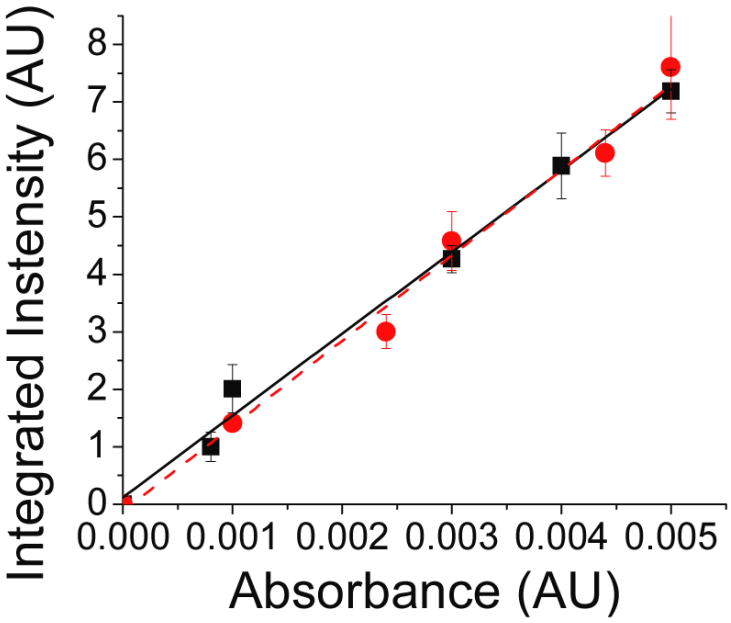

Figure 6.
Plots of integrated intensity versus absorbance for Rh6G (black squares) and DOSNPs (red circles) in DI water. The slopes of the linear fit (Rh6G: black line, DOSNP: red dashed line) were 1421.4 ± 63.4 and 1483.3 ± 77.9, respectively. The correlation coefficients (r^2) for integrated intensity versus absorbance were 0.9901 and 0.9863, respectively.

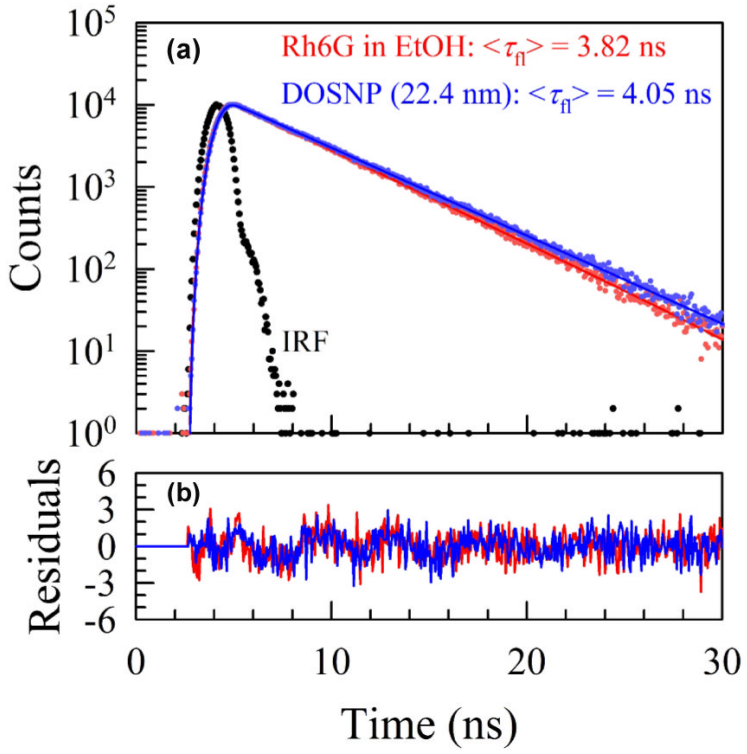

Figure 7.
(a) Typical excited-state intensity decay profiles for Rh6G dissolved in ethanol (red) and confeito-type Rh6G-containing suprananoparticles dispersed in water (blue). Solid lines show best fits to a single-exponential decay model. (b) Residuals between the data and the model. λ_{ex} = 458 nm; λ_{em} = 562 nm ($\Delta\lambda_{em}$ = 12 nm). The instrument response function (IRF) was measured with 80-nm colloidal SiO_2 dispersed in ethanol as scatterer.

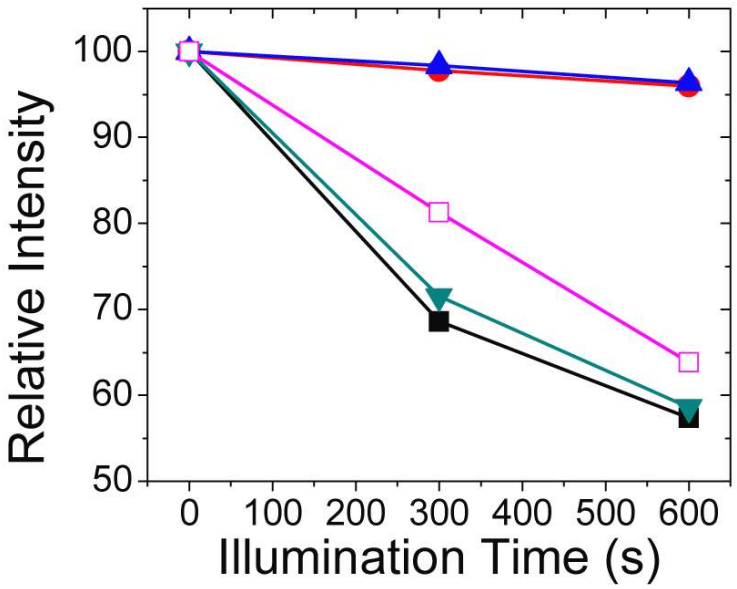

Figure 8.
Typical photodegradation decays of Rh6G (solid squares), 3.3 nm DOSNPs (upward triangles), 22 nm DOSNPs (circles), 3.3nm Rh6G adsorbed nanoparticle (empty squares) and 22 nm Rh6G adsorbed nanopartcles (downward triangles) under continuous illumination (475 nm/28 nm, 26 mW cm^{-2}).

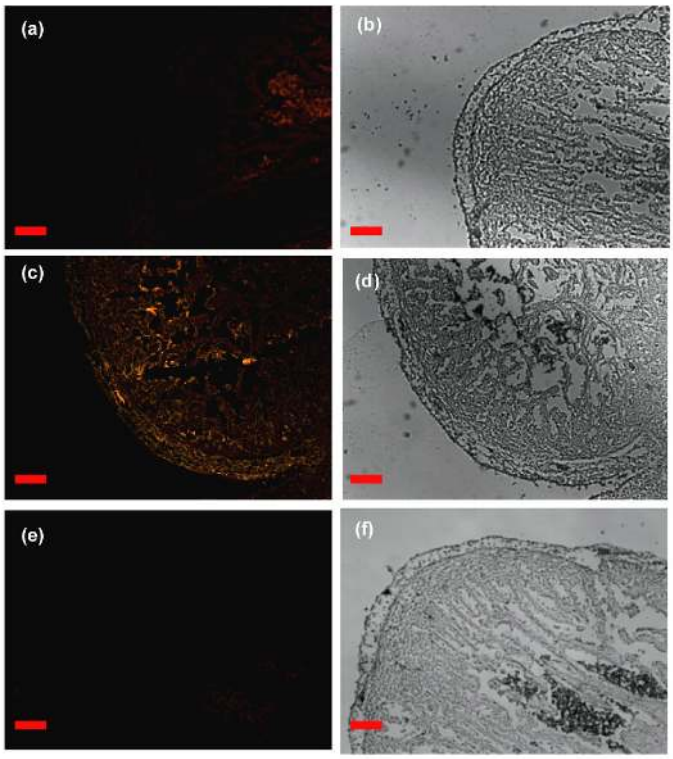

Figure 9.
Fluorescence and optical images of fibronectin in chick heart: (a) fluorescence and (b) optical images with Dylight 549 labeled antimouse antibody (antibody concentration: 3 nM), and (c) fluorescence and (d) optical images with Rh6G DOSNP labeled antimouse antibody (antibody concentration 3 nM) are shown. In both cases primary antifibronectin antibodies are raised in a mouse. As control samples, (e) fluorescence and (f) optical images with DOSNPs (no antibody) are shown. Images are taken with a bandpass excitation filter (543 nm center, 22 nm halfwidth) and a long pass emission filter (50% T @ 575nm), 300 ms exposure; scale bar 10 μm.

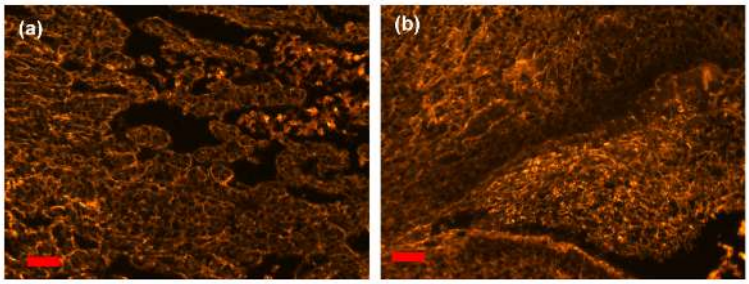

Figure 10.
Fluorescence images of fibronectin in chick heart. (a) DyLight 549 labeled antimouse antibody, (b) Suprananoparticle labeled antimouse antibody. Concentrations of labeled antibodies are 1900 and 3 nM for (a) and (b) respectively. The experimental conditions are the same as in Figure 6 but with lower magnification (scale bar 20 μm); exposure time 617 ms.